Science Advances
AAAS

advances.sciencemag.org/cgi/content/full/4/9/eaat0626/DC1

Supplementary Materials for

Transparent arrays of bilayer-nanomesh microelectrodes for simultaneous electrophysiology and two-photon imaging in the brain

Yi Qiang, Pietro Artoni, Kyung Jin Seo, Stanislav Culaclii, Victoria Hogan, Xuanyi Zhao, Yiding Zhong, Xun Han, Po-Min Wang, Yi-Kai Lo, Yueming Li, Henil A. Patel, Yifu Huang, Abhijeet Sambangi, Jung Soo V. Chu, Wentai Liu, Michela Fagiolini*, Hui Fang*

*Corresponding author. Email: h.fang@northeastern.edu (H.F.); michela.fagiolini@childrens.harvard.edu (M.F.)

Published 5 September 2018, *Sci. Adv.* **4**, eaat0626 (2018)
DOI: 10.1126/sciadv.aat0626

The PDF file includes:

Fig. S1. Bilayer-nanomesh structure and transmittance study.
Fig. S2. Bilayer-nanomesh microelectrode demonstration.
Fig. S3. Impedance results from different bilayer-nanomesh MEAs.
Fig. S4. Bench-top sine wave signal recording.
Fig. S5. Light-induced artifact characterization.
Fig. S6. Demonstration of artifact-free, ITO/PEDOT:PSS bilayer-nanomesh microelectrodes.
Fig. S7. Artifact rejection and wireless recording system.
Fig. S8. Artifact rejection using Au nanomesh microelectrode.
Fig. S9. Histology studies.
Fig. S10. In vivo transparency of MEA.
Fig. S11. Optical imaging underneath microelectrode.
Fig. S12. In vivo impedance measurement after implantation.
Fig. S13. Optimization of nanosphere lithography.
Legends for movies S1 to S5

Other Supplementary Material for this manuscript includes the following:

(available at advances.sciencemag.org/cgi/content/full/4/9/eaat0626/DC1)

Movie S1 (.mp4 format). Wide-field epifluorescence of the Ca^{++} indicator GCaMP6s showing the activity in the superficial layers of the mouse visual cortex and the surrounding areas (30× faster than the real time).
Movie S2 (.mp4 format). Video-rate two-photon Ca^{++} imaging from the neurons of the layer 2/3 of the mouse visual cortex expressing the Ca^{++} indicator GCaMP6s (30× faster than the real time).

Movie S3 (.avi format). Correlation between the $\Delta F/F$ of Ca^{++} wide-field epifluorescence and the MEA recording (30× faster).
Movie S4 (.mp4 format). The correlated response of arousal (left), the map of the modulation of the power of the MEA recording in different electrophysiology frequency bands (center), and the $\Delta F/F$ of the two-photon Ca^{++} imaging (right) (3× faster than the real time).
Movie S5 (.mp4 format). Map of the modulation of the power of the MEA recording in the multi-unit band (300 Hz to 7 kHz) during the alternation of visual stimuli and isoluminous gray screen presentations (3× faster than the recording) in which evoked cortical activity (higher, color-coded in red) alternates with spontaneous cortical activity (lower, color-coded in green) based on the stimulus/nonstimulus presentation.

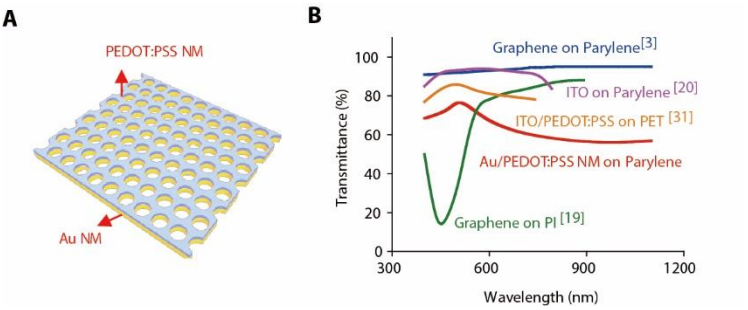

Fig. S1. Bilayer-nanomesh structure and transmittance study. (**A**) A model illustrating the bilayer nanomesh structure. The thickness is 25 nm for Au and 85 nm for PEDOT:PSS. (**B**) Transmittance spectra of Au/PEDOT:PSS nanomesh and other transparent ones in literature.

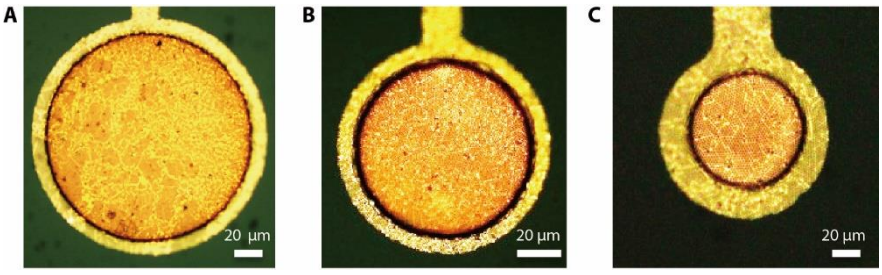

Fig. S2. Bilayer-nanomesh microelectrode demonstration. Microscope images of Au/PEDOT:PSS nanomesh microelectrodes with (**A**) 140 μm, (**B**) 80 μm, (**C**) 40 μm.

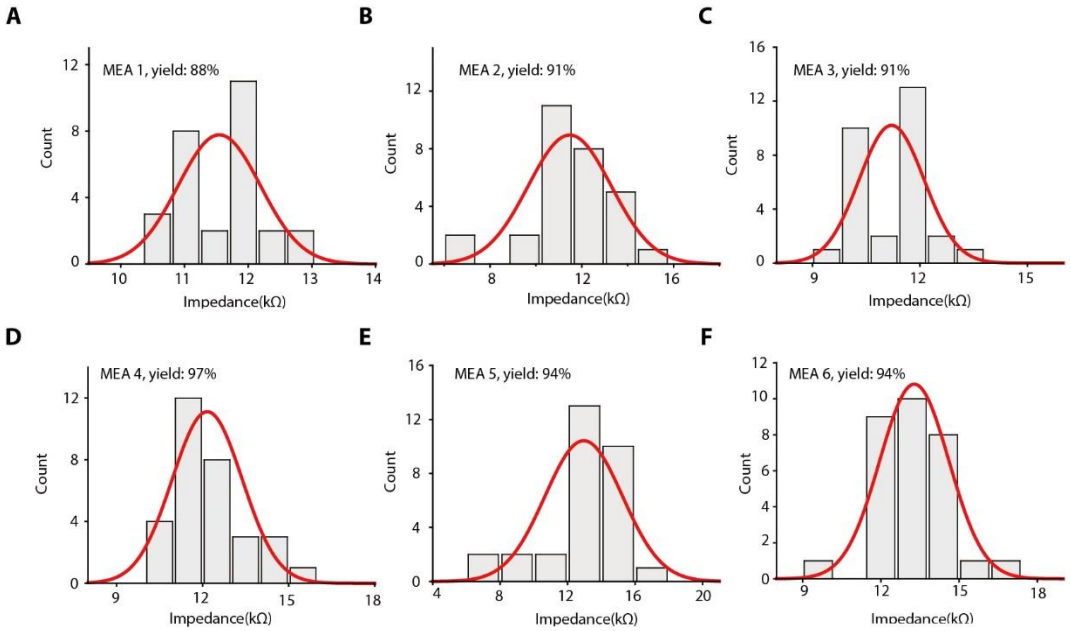

Fig. S3. Impedance results from different bilayer-nanomesh MEAs. Impedance histogram of Au/PEDOT:PSS nanomesh microelectrode arrays: (**A**) MEA #1, (**B**) MEA #2, (**C**) MEA #3, (**D**) MEA #4, (**E**) MEA #5 (**F**) MEA #6.

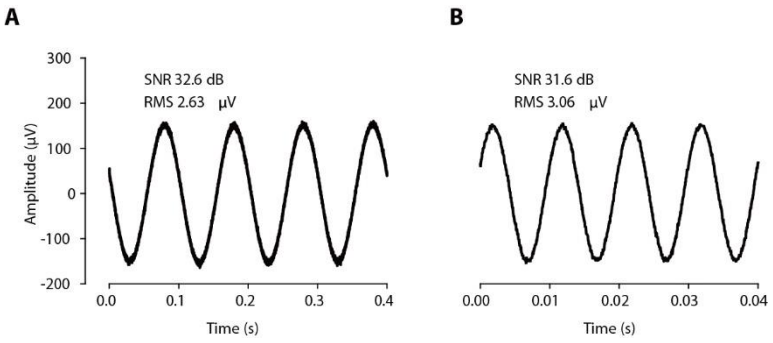

Fig. S4. Bench-top sine wave signal recording. Recording using Au/PEDOT:PSS nanomesh MEA with sinewave signals of 316 $\mu V_{p\text{-}p}$ at (**A**) 10 Hz, (**B**) 100 Hz

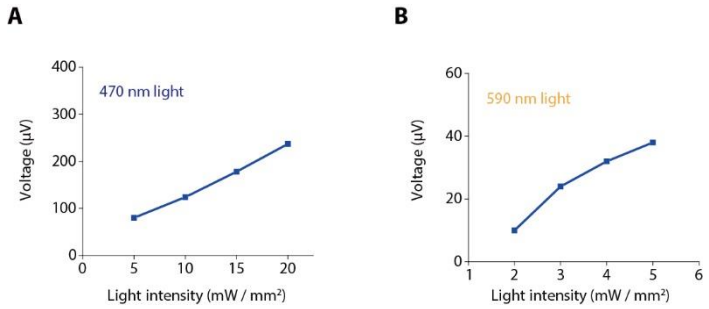

Fig. S5. Light-induced artifact characterization. Artifacts from Au/PEDOT:PSS nanomesh MEA using (**A**) 470 nm blue night (**B**) 590 amber light.

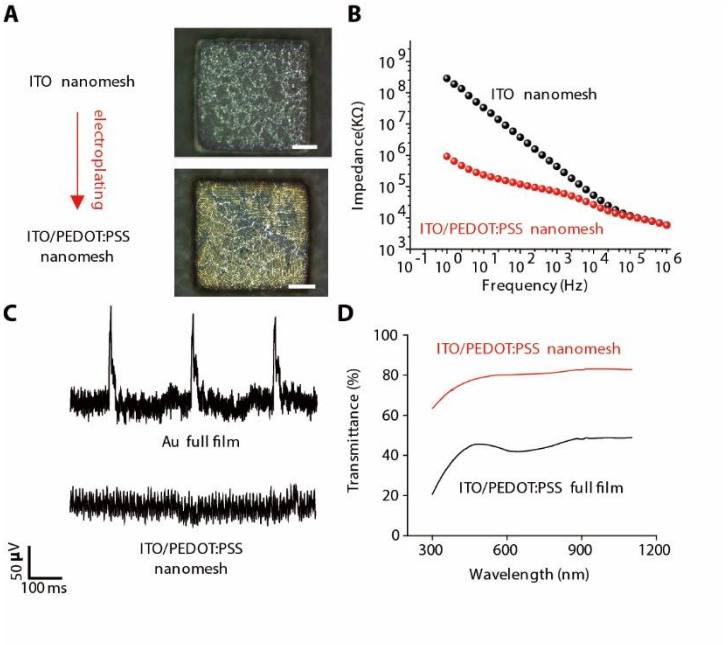

Fig. S6. Demonstration of artifact-free, ITO/PEDOT:PSS bilayer-nanomesh microelectrodes. (**A**) *Top*: ITO nanomesh microelectrode; *Bottom*: ITO/PEDOT:PSS nanomesh microelectrode (scale bar: 20 μm). (**B**) Impedance magnitude of ITO nanomesh and ITO/PEDOT:PSS nanomesh microelectrodes. (**C**) Noise recording with 470 nm, 5 Hz (5 ms duration) blue light shining on microelectrodes with an intensity of 20 mW/mm^2: *Top*: Au full film microelectrode; *Bottom*: ITO/PEDOT:PSS nanomesh microelectrode. (**D**) Transmittance spectra of *Left*: ITO/PEDOT:PSS; *Right*: ITO/PEDOT:PSS nanomesh microelectrodes.

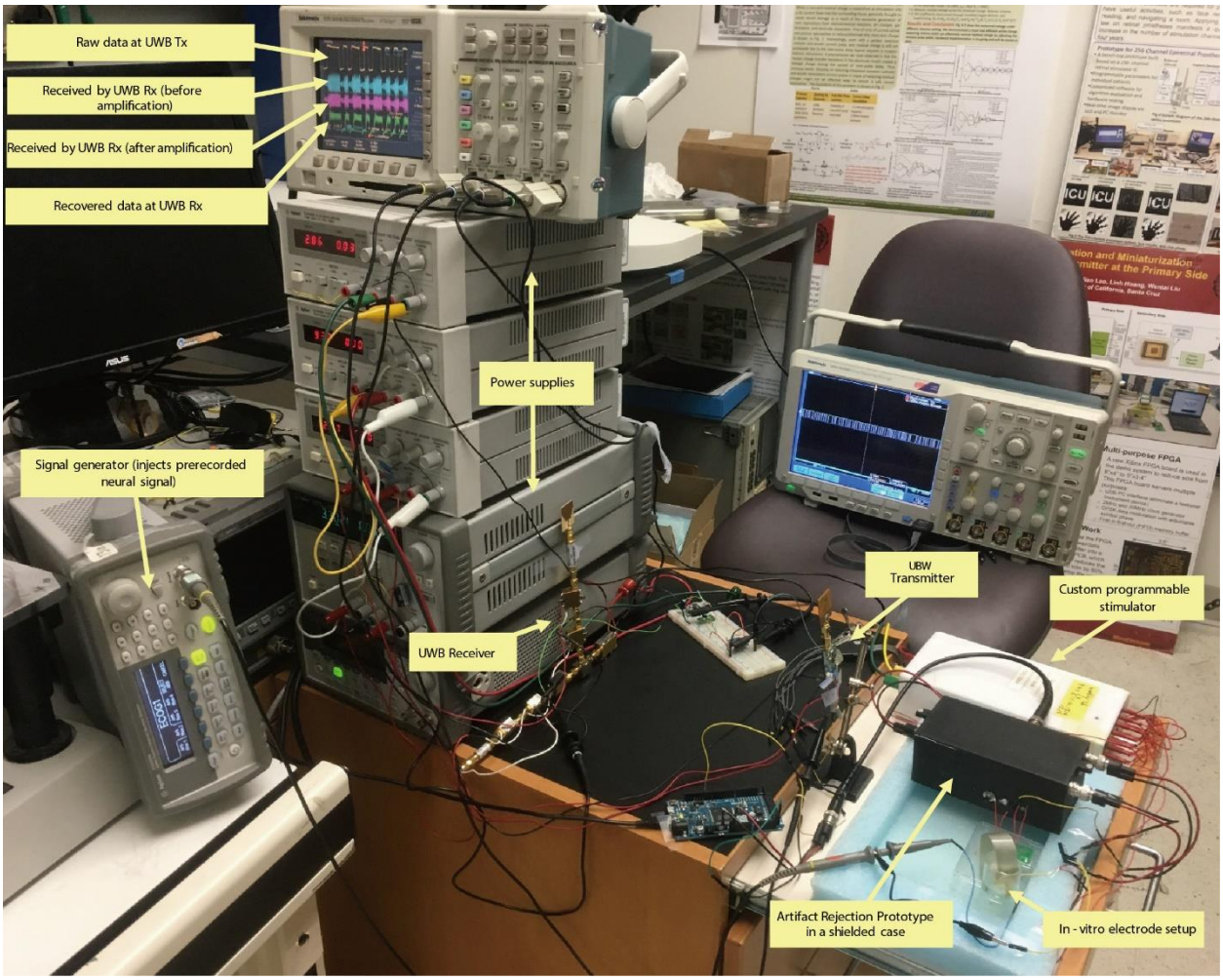

Fig. S7. Artifact rejection and wireless recording system. Physical test setup for demonstration of concurrent neural recording and stimulation with the 32-channel Au/PEDOT:PSS nanomesh MEA using an amplifier front-end with online stimulation artifact rejection and a back-end UWB wireless transmitter. Photo credit to Biomimetic Research Lab, UCLA.

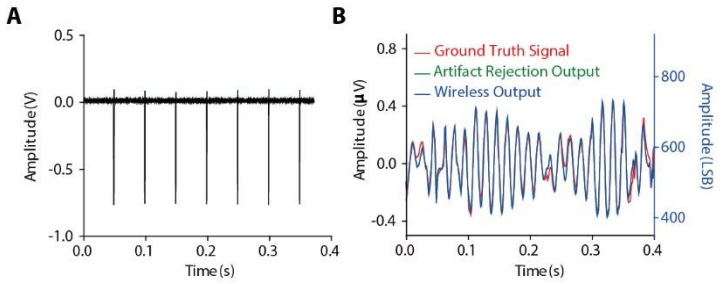

Fig. S8. Artifact rejection using Au nanomesh microelectrode. Artifacts rejection using pure Au nanomesh microelectrode: (**A**) Input neural signal contaminated with large stimulation artifacts (Stimulation current: 0.05 mC/cm^2). (**B**) Ground truth neural signal overlapped with artifact rejection output (*Left y-axis*) and wireless output (*Right y-axis*) for comparison.

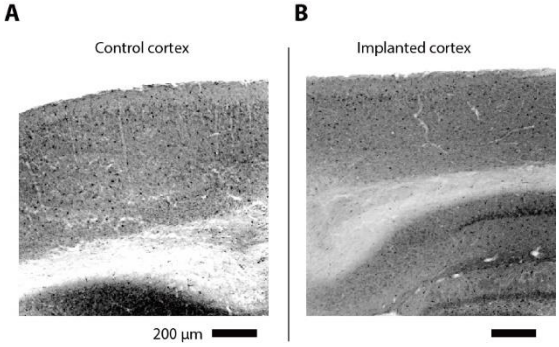

Fig. S9. Histology studies. IBA1 staining for evaluating possible microglia activation on the control cortex (**A**, control) and on the cortex implanted with both cranial window and transparent MEA (**B**, electrode only).

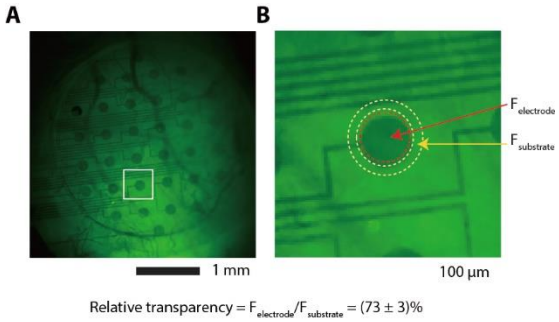

Fig. S10. In vivo transparency of MEA. *In vivo* optical measurement showing relative transparency between Au/PEDOT:PSS nanomesh microelectrode site and Parylene C substrate (**A**, zoomed out, **B**, zoomed in.)

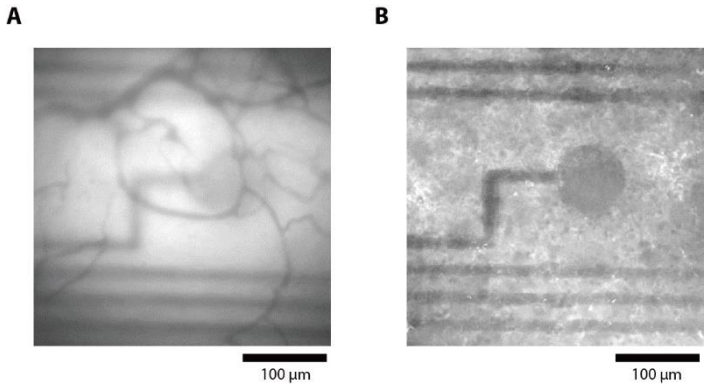

Fig. S11. Optical imaging underneath microelectrode. Average epifluorescence Ca^{++} imaging (**A**) and 2-photon Ca^{++} imaging (**B**) on dendrites in layer I (depth < 50 µm). The size of the electrode pad (diameter = 80 µm) is less than the imaged depth in layer I. The Ca^{++} sensor GCaMP6s has been imaged with conventional FITC filters for epifluorescence (1-photon excitation) and with 930 nm pulsed excitation, 500-550 nm emission filter for 2-photon imaging (2-photon excitation).

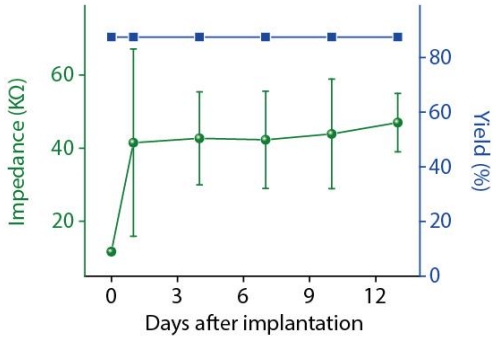

Fig. S12. In vivo impedance measurement after implantation. *In vivo* impedance measurement with days after implantation: *Left*: Impedance value at 1 KHz; *Right*: MEA Yield with days after implantation.

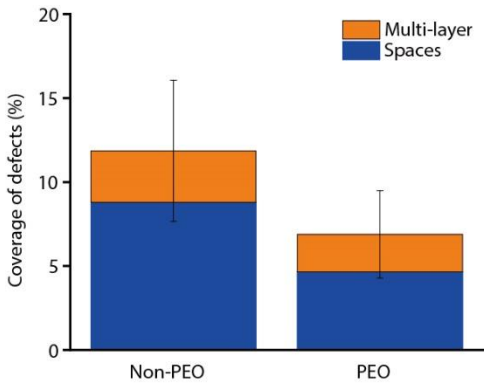

Fig. S13. Optimization of nanosphere lithography. Coverage percentage of nanosphere defects (multiplayer or empty space) with and without PEO added to PS nanosphere solution.

Supplementary Movies

Movie S1. Wide-field epifluorescence of the Ca^{++} indicator GCaMP6s showing the activity in the superficial layers of the mouse visual cortex and the surrounding areas (30× faster than the real time).

Movie S2. Video-rate two-photon Ca^{++} imaging from the neurons of the layer 2/3 of the mouse visual cortex expressing the Ca^{++} indicator GCaMP6s (30× faster than the real time).

Movie S3. Correlation between the $\Delta F/F$ of Ca^{++} wide-field epifluorescence and the MEA recording (30× faster). The white square indicates the position of the MEA.

Movie S4. The correlated response of arousal (left), the map of the modulation of the power of the MEA recording in different electrophysiology frequency bands (center), and the $\Delta F/F$ of the two-photon Ca^{++} imaging (right) (3× faster than the real time). The white squares indicate the area imaged by the 2-photon microscope.

Movie S5. Map of the modulation of the power of the MEA recording in the multi-unit band (300 Hz to 7 kHz) during the alternation of visual stimuli and isoluminous gray screen presentations (3× faster than the recording) in which evoked cortical activity (higher, color-coded in red) alternates with spontaneous cortical activity (lower, color-coded in green) based on the stimulus/nonstimulus presentation.